PBAR PRODUCTION AND COLLECTION AT THE FNAL ANTIPROTON SOURCE

G. Dugan
Fermi National Accelerator Laboratory*
P.O. Box 500, Batavia, IL USA 60510

Summary

The design, implementation, commissioning and future of the FNAL Antiproton Source target station and pbar collection system will be discussed. The design and operation of the principal target station components will be presented. Results from the first commissioning period of the Antiproton Source will be compared with design expectations. Finally, the direction of future improvements will be indicated.

Introduction

The FNAL Antiproton Source is the accelerator complex in which antiprotons are produced, collected and stored for use in the operation of the FNAL Tevatron as a -p collider. The principal components of this accelerator complex[1] are two storage rings (Debuncher and Accumulator), four beam lines and a target station. The production and collection of the antiprotons takes place in the target station. The layout of the Antiproton Source is shown in fig. 1.

To produce antiprotons, one booster batch of about 2×10^{12} protons is accelerated in the FNAL Main Ring once every two seconds and extracted in a single turn at F17[2]. They are transported along a 174 m long beam line (called AP-1)[2,3] and focussed onto a tungsten-rhenium production target using a series of 4 pairs of quads at the end of AP-1. The resulting secondaries are collected by a 15 cm long, 2 cm diameter lithium lens, which does a point-to-parallel focus from the target into a 300 m long conventional secondary beam line (called AP-2)[4]. The first element of this line is a pulsed magnet, which separates 8 GeV negative secondaries from the positive primary beam, which is delivered to a beam dump. The negative secondaries are transported along the AP-2 line and injected into the Debuncher. The total flux which the pbar production and collection system is designed to handle is determined by the transverse and longitudinal acceptances of the Debuncher, which are respectively 20π mm-mrad and ±2% in momentum. The design flux is 7×10^{7} antiprotons per 2×10^{12} protons on target, at a cycle rate of 0.5 Hz.

Target Station

The Antiproton Source target station[5] contains the antiproton production target, the lithium lens, the pulsed magnet, and the proton beam dump, together with collimators and associated instrumentation.

These target station components are all contained in a small volume surrounded by shielding in an area called the target station vault. The layout of the vault is shown in fig. 2. The volume occupied by the components is 0.8m wide, 1 m high and 4.1 m long. It is surrounded by 1.3 m of steel to the sides and bottom, and 1.8 m of steel plus 0.3 m of neutron absorbing borated wax to the top. Each component is individually hung from a 1.8 m long block of steel immediately above it called a "module". Modules can be lifted out and replaced like vertical drawers with a crane. The modules can be moved to a storage or work area (the alcove) inside the vault. Viewing through the shielding wall is provided by thick lead-glass windows in the wall.

The modules and their linkages to the target station components which they support are designed in such a way that, when placed in the alcove with the crane, a used component can be removed from the module, and a new component attached, by personnel working entirely outside the vault area. Thus, components can be changed with a minimum of radiation exposure. An alignment system, based on two shielding plates 1.8 m deep acting as stiff support rails (see fig. 2), allows precise relocation (to better than 1 mm) of the components when a module is removed and replaced.

The target station vault is housed in a large building called the Target Service building. This building also houses the power supplies associated with the pulsed components, and the electronics for the instrumentation and control of the supplies. Hatches at the upstream and downstream end of the building allow access to the AP-1 and AP-2 beam lines. Dehumidification and circulation of the air within the target station component volume is achieved using a special air handling unit. This volume is maintained at a lower pressure than the building above to prevent escape of radioactive gases and dust. The air is swept along AP-1 and exhausted to the outside after a holding time of 20 minutes.

Target Station Components

Instrumentation

The principal instrumentation in the target station consists of a high-resolution wire secondary emission profile monitor[6] and a beam position monitor. The purpose of the beam profile monitor, which is located just upstream of the target, is to measure the size of the proton beam on target, which is very important in determining the yield of secondaries from the target. The beam position monitor (a capacitive pickup) provides information on the beam centroid, which is useful in maintaining the centroid on the lens optic axis.

The secondary emission monitor provides beam shape information in both planes. A typical beam profile measurement is shown in fig. 3. The bin size, which is equal to the monitor wire spacing, is 0.25 mm. The profile monitor is read out directly by the accelerator control system, providing a real time display similar to figure 3. Proton beam intensity information is provided by a standard current toroid located upstream of the target station vault.

Target

The target assembly is a series of horizontal tungsten-10% rhenium discs produced by powder technology (see fig. 4). The heary metal discs are separated by copper discs with channels for the passage of pressurized air. The air is fed through the target mounting shaft to the channels to remove

*Operated by Universities Research Association, Inc. under contract with the U.S. Department of Energy.

the heat deposited by the beam (about 200 watts). The entire target disc assembly is housed in a thin titanium cylinder to contain any fragmentation of the discs which may occur.

The target disc assembly is positioned relative to the proton beam such that the beam subtends a chord of the disc; transverse motion of the vertical disc axis perpendicular to the beam allows the effective length of the target to be changed; vertical motion of the assembly allows the target disc illuminated by the beam to be changed, or the target to be removed completely from the beam. The target discs can also be rotated about their vertical axis between beam pulses, minimizing the potential damage to any one area of the target disc.

The three target motions described above are all provided by remotely operated drive mechanisms at the top of the module. Recently, a new module has been designed in which the target will be mounted on a horizontal pivoting arm, allowing target motion of a few centimeters along the beam direction to be accomodated by a rotation of the horizontal arm about a vertical axis through the module. This will allow remote optimization of the target-lens distance, a feature not possible in the earlier design.

The choice of tungsten-10% rhenium for the target material results from several considerations. Because of the small depth-of-field of the short focal length lithium lens (f* = 14.5 cm), a high density material is mandatory. For a given proton beam intensity, to maximize the antiproton transverse density at production, the smallest feasible proton spot size is desirable. However, as the proton spot size is reduced, the peak energy density deposited by the beam rises. This results in severe instantaneous thermal stresses in the target[7], as well as the development of shock waves. The target material should thus be as resistant as possible to thermal stress. Tungsten-10% rhenium is a favorable choice from the point of view of susceptibility to thermal stress, since this alloy exhibits a higher yield stress than tungsten at elevated temperatures.

Lithium lens/transformer system

The development of the FNAL lithium lens and transformer system benefited enormously from the pioneering work done at the INP in Novosibirisk[8]. The application of a lithium lens as a collection device for the Antiproton Source required the development of a large (2 cm) diameter lens, operating at a gradient of about 1000 T/m. The development of large diameter lenses has also been underway simultaneously at other laboratories[9]. To achieve this gradient, the Fermilab lens is pulsed to a peak current of about 650 kA. The current pulse is a half-sine wave of duration 360 microseconds, giving a value for the current penetration ratio (δ/R_0) = (skin depth/ radius) of about 0.45. With this value for the ratio, the optimum phase[10] is about 120°. In operation with beam, the timing of the lens current pulse is adjusted such that the beam (of duration 1.6 microseconds) passes through the lens at the optimum phase, when the lens current is about 500 kA and the gradient is about 1000 T/m.

The mechanical and electrical design of the lens and its toroidal transformer have been described in ref. 11. The assembly and filling procedure, and the first power test, were described in ref. 12.

Since the publication of the above papers, several modifications have been made to the lens as a result of the testing program. After about 10^4 pulses at full power (lens peak current 650 kA), and at full repetition rate (0.5 Hz), failures of the 8 high-strength steel bolts which contain the lens end flanges against the axial forces occurred. These bolts are shown in fig. 5, which illustrates the lens design. The failures were due to fatigue of the bolts. The bolts were replaced with titanium (Ti 6A1-4V) bolts, with special care being taken in the thread and bolt shape design to enhance fatigue resistance. No bolt failures have been observed since the change was made to titanium bolts.

After about 3×10^4 pulses in one lens, and about 8×10^4 in another, failures in one of the internal welds in the lens occurred. This was the weld joining the outer radius of the titanium water septum with the titanium plenum (see fig.5). Again, this failure was fatigue-initiated; it was determined that the failue was due to pulsed loads transmitted to the water septum from the inner wall of the titanium jacket through the water. The septum design in this area was revised to strengthen the weld. Since then, two lenses have each reached 3×10^5 pulses without failures. In each case, the testing was terminated due to failures of the toroidal transformer.

The toroidal transformer has an 8-turn primary and a single-turn secondary; the secondary is the aluminum housing around the tape-wound core, which is completed by the lens itself when it is inserted into the center of the transformer. To develop the required secondary current for full power lens operation, the primary current required is about 80 kA. The details of the transformer design are discussed in refs 11 and 12. The lens is attached to the transformer secondary by a clamping device. The choice of a removable connection between the lens and transformer was made to allow for the possibility of separation of a radioactive lens/transformer system (using remote manipulation techniques) to salvage one of the components.

One of the transformer failures mentioned above, which occurred after about 300,000 pulses, was a fatigue failure of the secondary (aluminum) housing near the inner diameter of the area facing the core. The thickness of this section has been increased in the present design. The other failure was due to the lens-transformer clamp, the material of which had not been properly hardened before use.

Pulse testing of the present design of the lens-transformer system will resume this summer and be pursued until lifetimes of several million pulses are acheived. The present version of the transformer is only semi-radiation-hard (torlon and kapton, plastics, are used as insulators); a design for a radiation-hard version, based on all-ceramic insulation, is under development.

In the target station vault, the lens-transformer system is suspended from a module (see fig. 6). The current pulse is delivered to the transformer via a strip line which runs along the side of the module. Remote adjustment of the position and angle of the lens is possible using motor drive mechanisms mounted on the module; these position and angle controls are interfaced to the accelerator control system, allowing real-time optimization. The lens is cooled by a closed loop water system (10 kW capacity) equipped with a deionizer. This system resides outside the target vault, and contains automatic sensors to detect a breach of the water jacket during operation (which causes an automatic purge of the lens with argon).

Pulsed Magnet

The original design for the pulsed magnet, which defines the secondary beam energy, was a 6-turn magnet, with a gap of 3.8 cm and a length of 30 cm. When pulsed to about 80 kA, the magnet developed a field of about 5 T; this was sufficient to provide the required 3° bend for 8 GeV secondaries. A semi-radiation-hard version of this magnet was designed, fabricated and tested. Problems were encountered with the turn-to-turn insulation in the magnet; after several tens of thousands of pulses, the insulation separating the turns failed near the end of the magnet.

Because of these problems, this magnet has been replaced with a more conventional design magnet. The new magnet is about 1 m long, with a 3-8 cm gap and 200 turns. It is pulsed to about 450 A, developing a field of about 1.5 T. The additional length of this magnet requires the use of 4 modules to allow for remote handling capabilities. The magnet is also not radiation-hard. In the future, it is planned to replace this magnet with a shorter device, having fewer turns and a higher current and field, which can be more easily radiation-hardened.

Proton beam dump

The proton beam dump is similar in design to the Tevatron dump. The dump core contains a 15 cm diameter, 1.2 m long graphite cylinder, enclosed in an aluminum container. The graphite is followed downstream by 1.1 m of aluminum. The dump is water cooled by a closed loop system of 80 kW capacity. The water circulates through channels in the aluminum enclosure.

The core is surrounded by shielding steel. A channel through the steel is necessary to allow the 8 GeV secondaries to exit the downstream wall of the dump. This channel contains a remotely operated beam stop (see fig. 2) which blocks the secondary beam when necessary for radiation safety purposes.

Yield Estimates

Estimates of the yield (Y) of pbars, defined as

Y = flux of 's/flux of protons/momentum spread,

and measured in ppm(=parts per million)/Gev/c, have been made using Monte Carlo techniques for the FNAL Antiproton Source[13]. These estimates were used to determine the operating parameters of the pbar production and collection system. The dependence of the yield on the operating parameters can be seen from fig. 7, which displays the yield Y vs the aspect ratio β_0 of the pbar collection system's upright acceptance ellipse at the target center, for various acceptance areas. Fig. 7 was computed by a semi-analytical technique described in ref. 14, which is based on the formalism developed in ref 15. The pbar production cross section parameterization was taken from ref. 13. Although multiple scattering and secondary production are not included, these effects come in at the 10-15% level in determining the yield; the results shown in fig. 7 agree with the Monte Carlo calculations of ref. 13 at this level. The dependence of the yield on the lens parameters can be seen from the relation

$$\beta_0 = \frac{1}{\beta_l k^2 \sin^2\Phi}$$

where β_l = beta at the lens exit $=R_0^2/(a/\pi)$, R_0 = lens radius, a = system acceptance; $k^2 = eG/p$ = lens strength, and $\Phi = kl$ = lens phase advance (l = lens length). For the FNAL system, R_0 = 1 cm, a = 20π mm-mrad, so β_l = 5 m; G = 1000 T/m, ρ = 8.9 GeV/c, so $k = 5.8\ m^{-1}$, Φ = .87 radians, so β_0 = 1 cm. This is near the peak of the yield vs β_0 curve shown in fig. 7 for a = 20π mm-mrad; the system is thus designed to operate near the optimum point, and the yield should not be very sensitive to variations in any of the lens parameters.

Secondary Beam Transport

The 8 GeV negative secondary beam, which is selected by the pulsed magnet, is transported to the Debuncher along a 300 m long beam transport line called AP-2[4]. The beam line is designed to transport 20π mm-mrad of transverse emittance, and ±2.5% of momentum spread, from the lithium lens to the Debuncher; and to match the lattice functions from the exit of the lens (where beta is about 5 m) to injection into the Debuncher.

The beam line has been instrumented heavily in order to enhance understanding of the optics and to aid in the diagnosis of problems. 6 secondary emission monitors have been provided to allow measurement of the beam profile at strategic points. An ion chamber (called IC728) has been installed in the beam line, about 42 m upstream of the Debuncher injection point; this chamber allows the determination of the absolute yield of negative secondaries at this point in the beam line. At this same location, during the last run (see below), a Cerenkov counter was temporarily installed to allow determination of the relative pion and antiproton yields.

Target Station Performance

During the period of the first commissioning of the Antiproton Source, which occurred during the spring, summer and early fall of 1985, a number of measurements were made relevant to the performance of the pbar production and collection system. Flux measurements were made in the downstream portion of AP-2 (at IC728), and measurements of the circulating beam in the Debuncher were made. The results of these measurements are detailed in ref. 16. Previous beam tests of the Fermilab lithium lens have also been reported[17].

The most significant measurement, as far as the operation of the Antiproton Source is concerned, is the determination of the absolute yield of pbars. The total secondary yield at the ion chamber IC728, relative to the number of protons on target, was measured to be 1.2×10^{-3} (with about 10% errors). The relative number of pbars to total secondaries at this point was measured with the Cerenkov counter to be 3.2% (again, with about 10-15% errors). Estimating the momentum acceptance of the AP-2 line to be about 4.8% gives the result for the pbar yield shown in fig. 8. Also shown in the figure is the corresponding yield for the circulating antiproton beam in the Debuncher. The curves plotted in fig. 8 are the predicted variation in yield with system acceptance, for the operating parameters under which the data were taken. The yield measurements have been located along the ordinate to lie near the curves. If the calculation (which follows the technique of ref 14) is correct, then the measurements allow us to infer an effective system acceptance at IC728 and in the Debuncher. The acceptance at IC728 is about 13π mm-mrad; this is

substantially smaller than what is expected at this point, which is well in excess of 20π mm-mrad. The Debuncher acceptance is close to 5π mm-mrad; the design acceptance is 20π mm-mrad, and measurements of the acceptance with proton beams have indicated acceptances in the vicinity of 10 to 12π mm-mrad. The small effective acceptance shown in fig. 8 probably results from emittance dilution due to both poor matching and injection oscillations in the Debuncher.

During studies performed in the early part of 1986, the Debuncher acceptance has been improved to better than 20π mm-mrad in both planes. The AP-2 beam line and injection diagnostics have been improved to help diagnose the problems contributing to the poor performance discussed above. During the next operating period of the Antiproton Source (fall 1986), the measurements discussed above will be continued, and determined efforts made to understand and eliminate the problems.

Extensive relative yield measurements have also been made; these are detailed in ref. 16. Measurements were made of yield vs. lens gradient (with target-lens distance, fixed); yield vs. proton beam spot size; yield vs. target length; yield vs. lens vertical position; and yield vs. lens timing. In general, the relative yield measurements are all in rough quantitative agreement with calculations. As an example of the data, the yield vs. lens timing measurements are shown in fig. 9. The variation of the yield with lens timing is due primarily to the dependence of the lens field linearity on phase, and also to a lesser extent on the variation in the lens gradient with phase. In fig. 9, the measured relative total yield (at IC728) is shown, together with a measure of the lens linearity, Δ_{RMS}. Δ_{RMS} is the root mean square relative deviation of the lens field from linearity; the origin of the nonlinearity is discussed in detail in refs. 10 and 18. The minimum in Δ_{RMS} occurs at a time called the "optimum phase"; the nonlinearity is least here, and as fig. 9 shows, the yield peaks close to this point.

Future Improvements

In connection with possible upgrades of the Antiproton Source to handle higher fluxes, improvements to the pbar production and collection systems are being considered. These improvements are focussed on operation of the system at higher repetition rates than the present 0.5 Hz, and modifications to increase the pbar yield into a fixed acceptance (which requires an increase in the pbar transverse phase space density at production). Planning for these improvements is in an embryonic stage at present, but some of the directions which seem useful to pursue will be discussed below.

The repetition rate of the pbar production system is primarily limited by the cycle rate of the lithium lens. Reduction of the cycle time can be acheived by reducing the diameter of the lens. As detailed in ref 19, the temperature rise per pulse in the lens is

$$T_p T I_0^2 / R_0^4$$

where T is the pulse duration, and I_0 is the peak lens current. To acheive the same field linearity, the current penetration ratio (δ/R_0) should be kept constant, where $\delta\sqrt{T}$ is the skin depth. For constant $(\delta/R_0)^2$ T/R_0^2, T can decrease as R_0^2, so

$$T_p I_0^2 / R_0^2$$

Thus, to keep ΔT_p constant, I_0 must vary like R_0. The cyclic thermal stress in the lens cooling jacket (which is the overriding mechanical design constraint) is[19]

$$\Delta\sigma \quad \Delta T_p \quad f(R_0/t)$$

where f(x) depends on the lithium and jacket material constants, and t is the thickness of the cooling jacket. If ΔT_p is constant, $\Delta\sigma$ can be kept constant if (R_0/t) is maintained fixed as R_0 decreases. The minimum lens cycle time is proportional to the thermal time constant for heat transport across the jacket, τ_R:

τ_R tR_0

For constant R_0/t, $\tau_R R_0^2$; so, to reduce τ_R by a factor of 2 requires a reduction in R_0 (and I_0) by $\sqrt{2}$. Since the gradient will increase (as $1/R_0$), the focal length decreases; however, for operation at this reduced focal distance, the change in the pbar yield is very small (see fig. 10). Thus, to acheive factors of 2 or more improvement in the pbar production system cycle time, reduction of the lens radius from 1 cm to 7 mm or smaller is necessary; this change maintains the pbar yield and the principal mechanical stresses in the lens constant, and should be techically quite feasible to accomplish.

Improvements in the pbar transverse density at production are considerably more difficult to achieve. Since the pbar density is conserved after production, increases in density can only be acheived at the target. The simplest improvement involves exploiting the rough equality between the proton and pbar beam spot sizes at the target. Reduction of the proton beam spot size increases the pbar transverse density. Figure 11 shows the dependence of the pbar yield into a fixed acceptance on the proton beam size. It is clear that substantial gains are possible from the present design point of σ_R = 0.54 mm; the limit due to multiple Coulomb scattering in the target and lens is at $\sigma_R \sim 0.1$ mm. However, there are limits on the energy density which can be deposited in the target[7], and the present Antiproton Source operating parameters ($\sigma_R \sim 5$ mm, $N_p = 2\times10^{12}$ protons) are close to these limits. Significant reduction in the proton spot size will require some technique for avoiding the single pulse destruction of the target. One of the simplest possibilities involves the implementation of sweeping systems[20] to distribute the energy deposited by the reduced spot size' beam over a larger region of the target. The implementation of such a system at the FNAL target station is now under active consideration.

Alternative techniques for increasing the pbar density involve the elimination of the target depth-of-field effects. One method is the use of a current-carrying target, in which the field produced by an axial current focusses the secondaries as they are produced. Complete elimination of the target depth-of-field effect (i.e., the target appears as a source of no extension) occurs when the aspect ratio of the collection system acceptance ellipse β_0 at the target, and the target focusing field strength k = $\sqrt{eG_t/p}$ (G_t/ = target gradient), are related by $\beta_0 = 1/k$

For reasonable values of β_0, this implies very large values for the target gradient (in excess of 100,000 T/m). The best that has been acheived in laboratory tests to date[21] is in the range of 20,000 T/m. Fig. 12 shows the yield variation with target gradient, for different target lengths and a fixed acceptance and proton spot size. The value of β_0 at the target center has in each case been chosen as that for which the yield is a maximum. The gains in yield over the yield at $G_t = 0$, in the range up to about 30,000 T/m, are no more than 15%. Further studies will be performed to check if longer targets made of lower density materials (which might also tolerate higher local beam energy densities) could afford any greater gains.

Another alternative technique for reducing the target depth-of-field effect is the use of multiple short targets, alternating with lenses to focus the secondaries. This idea has been discussed extensively in previous papers[15,22]. A brief consideration of this technique has been made for the FNAL Antiproton Source case; this preliminary estimate indicates that to make sufficient gains to justify the development effort, at least the attenuation in the lenses must be eliminated: i.e., plasma lenses[23] or some equivalent non-absorbing focussing device (not lithium lenses) must be used. Feasibility studies of this approach will continue to be explored.

Conclusion

The FNAL Antiproton Source pbar production and collection system has been described. A detailed discussion of the target station, together with its components, was presented. The current state of development of the lithium lens and transformer system has been detailed. Some results have been presented of measurements relevant to the performance of the pbar production and collection system. Finally, the direction of future improvements to the system has been indicated.

Acknowledgements

The design, fabrication, installation and commissioning of the FNAL Antiproton Source target station and its components has been a collaborative effort of a large number of Fermilab staff members over the past four years. In particular, major efforts have been made by C. Hojvat, J. Hangst, J. Krider and G. Biallas (now at CEBAF). Many of the developments discussed here have benefited greatly from conversations with our colleagues at INP in Novosibirisk and in the AA group at CERN.

References

1. "Design Report, Tevatron I Project", Sept. 1984 (Fermilab); J. Peoples, "The Fermilab Antiproton Source", IEEE Trans. on Nucl. Sci., Vol. NS-30, 1970 (1983); R. Shafer, "Overview of the Fermilab Antiproton Source", in Proc. of the 12th Int. Conf. on High Energy Ace., 24 (1983); G. Dugan, "Tevatron I: Energy Saver and Pbar Source", IEEE Trans. on Nucl. Sci., Vol. NS-32,5,1582 (1985).

2. G. Dugan et al., "Proton Extraction and' Transport for Pbar Production in Tevatron I", IEEE Trans. on Nucl. Sci., Vol. NS-32,5,3009 (1985).

3. E. Colton et al., "120 GeV Proton Transport for Antiproton Production in the Fermilab Tevatron I Project", IEEE Trans, on Nucl. Sci., Vol. NS-30,4,2818 (1983).

4. E. Colton, C. Hojvat, "A Design for Antiproton Collection and Beam Transport in the Fermilab Tevatron I Project", IEEE Trans. on Nucl. Sci., Vol. NS-30,4,2784 (1983).

5. C. Hojvat et al., "The Fermilab Tevatron I Project Target Station for Antiproton Production", IEEE Trans. on Nucl. Sci., Vol. NS-30,4,2815 (1983).

6. J. Krider, C. Hojvat, "A Multiwire Secondary Emission Beam Profile Monitor with 20 Micron Resolution", to be published in NIM.

7. Proceedings of the High Energy Targeting Workshop, Fermilab (1980)

8. B. F. Bayanov et al., "A Lithium Lens for Axially Symmetric Focusing of High Energy Particle Beams", NIM 190,9 (1981); B. F. Bayanov and G. Sil'vestrov, "Use of Lithium to produce a Strong Cylindrical Magnetic Lens", Zh.Tekh.Fiz.48, 160 (1978).

9. B. F. Bayanov et al., "The Investigation and Design Development of Lithium Lenses with Large Operating Volume", in Proc. of the 12th Int. Conf. on High Energy Acc, 587 (1983); P. Sievers et al., "Development of Lithium Lenses at CERN", IEEE Trans. on Nucl. Sci. NS-32,5,3066 (1985).

10. T. Vsevolozhskaya et al., "Optical Properties of Cylindrical Lenses", Zh.Tekh.Fiz.45, 2494 (1975).

11. G. Dugan et al., "Mechanical and Electrical Design of the Fermilab Lithium Lens and Transformer System", IEEE Trans. on Nucl. Sci., Vol. NS-30, 4, 3660 (1983).

12. G. Biallas et al., "Power Tests of the Fermilab Lithium Lens for Antiproton Collection", in Proc. of the 12th Int. Conf. on High Energy Acc.,591 (1983).

13. C. Hojvat, A. van Ginneken, "Calculations of Antiproton Yields for the Fermilab Antiproton Source", NIM 206,67(1983).

14. G. Dugan, "Antiproton Yield Calculations", pbar note 449, Fermilab (unpublished)

15. T. Vsevolozskaya, "The Optimization and Efficiency of Antiproton Production within a Fixed Acceptance", NIM 190, 479(1981).

16. G. Dugan, "Comparisons of yield calculations with data", pbar note 448, Fermilab (unpublished)

17. D. C. Fiander et al., "Beam Tests of a 2 cm Diameter Lithium Lens", IEEE Trans. on Nucl. Sci., NS-32,5,3063 (1985).

18. A. Lennox,"The Design Parameters for a Lithium Lens as an Antiproton Collector", IEEE Trans. on Nucl. Sci., NS-30,4,3663 (1983).

19. G. Dugan, "Limits to the Pulse Repetition Rate of a Lithium Lens", in Proc. of the 1984 Summer Study on Design and Utilization of the SSC, 321 (1984).

20. T. Vsevolozskaya et al., "The Proton Beam Steering System for an Antiproton Target Station using Lithium Lenses", Fermilab TM-1048 (1981) (unpublished); "A Sweeping System for Obtaining Secondary Bunches with Large Phase Space Density", G.E. Silvestrov, A.D. Chernyakin", INP Preprint 84-168, Novosibirsk (1984).

21. T.W. Eaton et al., "Conducting Targets for Pbar Production of ACOL: Past Experience and Prospects", IEEE Trans. on Nucl. Sci. NS-32, 5,3060 (1985); A. Ijspeert et al, "Assessment of Further Development of Pulsed Targets for ACOL", SPS/TBT/Tech note 86-3 (1986).

22. J. Maclachlan et al., "Pulsed High Current Optics for Pbar Production at 5.4 GeV/c", IEEE Trans. on Nucl. Sci. NS-28,3,2785 (1981); J. Maclachlan FN-334, Fermilab (1982) (unpublished)

23. W. Panofsky, W. Baker, "A Focusing Device for the External 350-MeV Proton Beam of the 184 inch Cyclotron at Berkeley", Rev. Sci. Inst. 21,5,445 (1950); E. B. Forsyth et al, "The Brookhave-Columbia Plasma Lens", IEEE Trans. on Nucl. Sci., NS-12,3,872 (1963); L. DeMenna et al, "Plasma Lens for the CERN Antiproton Source", CERN PS/84-13 (AA) (1984); J. Christiansen et al., "Studies of a Plasma Lens with Pseudo-spark Geometry for Application in High- Energy Particle Accelerators", CERN PS/84-10 (AA) (1984).

Discussion

В.В.Пархомчук. Какой уровень радиации набирается на мишени сразу же после сеанса и когда вы могли начать с ней работать?

G.Dugan. Immediately after exposure, the radiation level was several tens of rads/hour at one foot from the target. Although the target cracking shown here did not cause operations to stop, if a more serious failure occurred, the target could be changed in 2-4 hours.

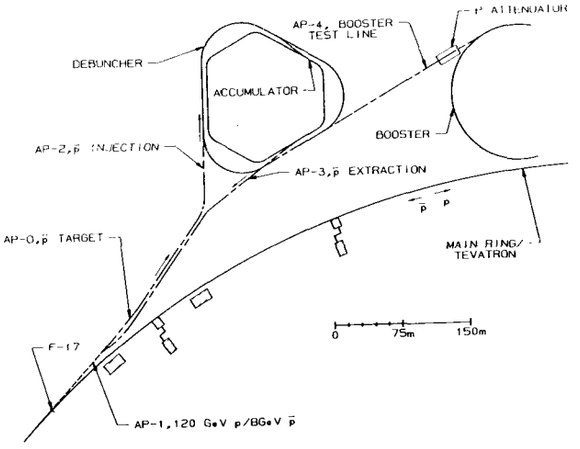

Fig. 1. Layout of the Antiproton Source

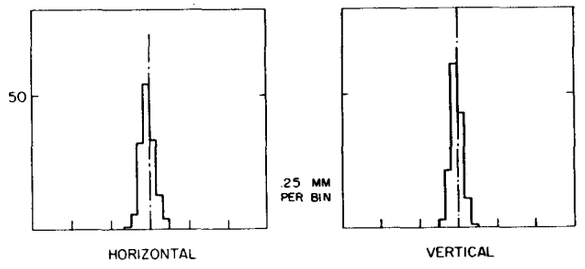

Fig. 3. Beam profile measurement of a single pulse of 120 GeV protons at the production target. Beam intensity was about 10^{11} per pulse.

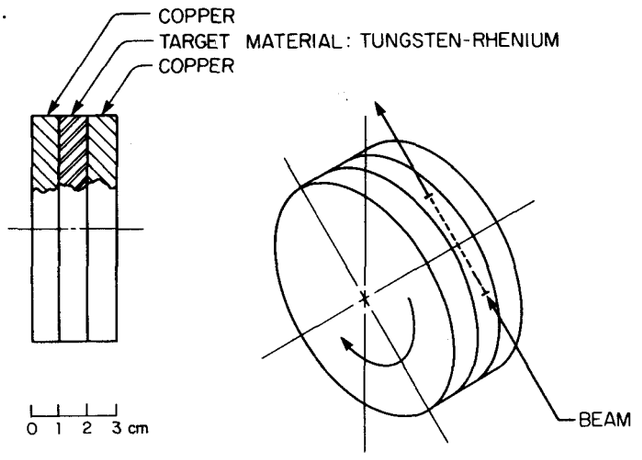

Fig. 4. Schematic of the target assembly. Air cooling channels and titanium housing are not shown.

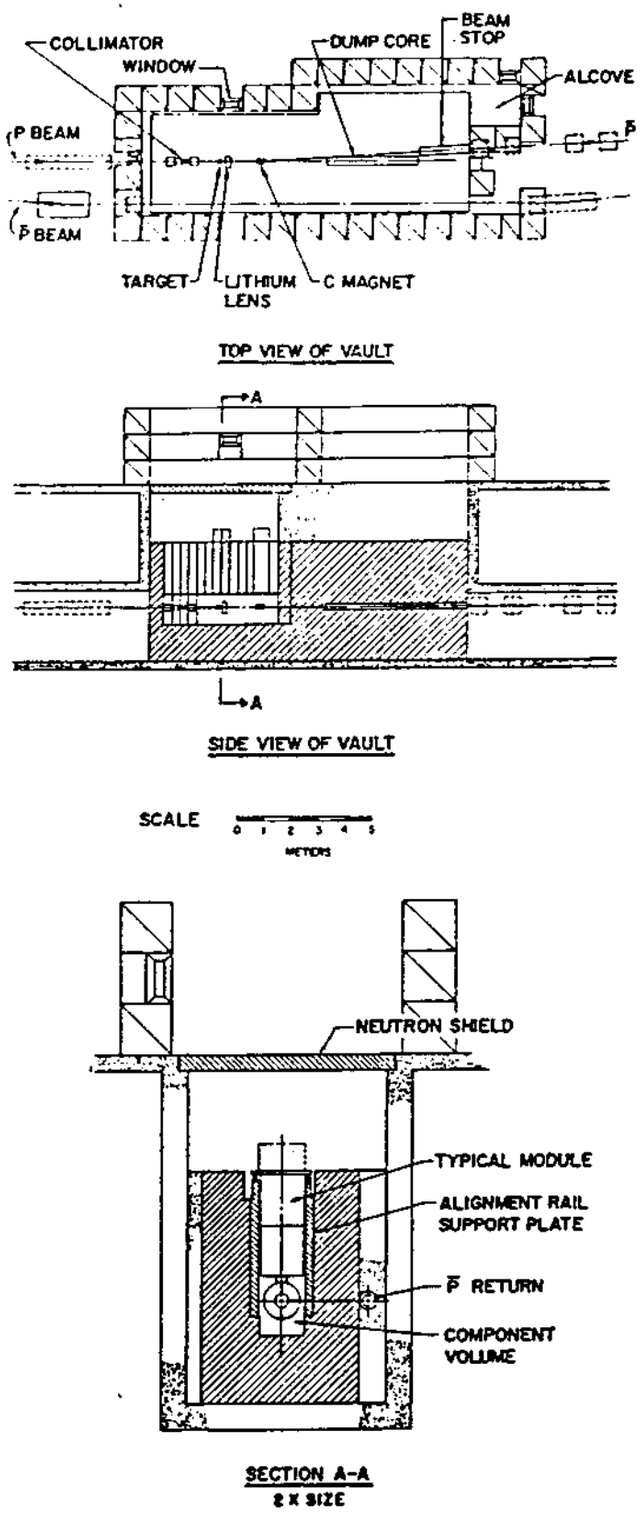

Fig. 2. Layout of the Target Station Vault

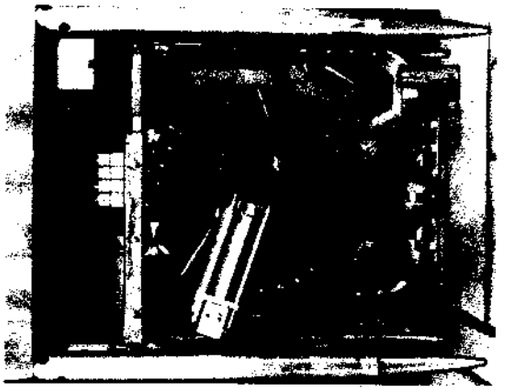

Fig. 6. Photograph of the lens-transformer system attached to the module.

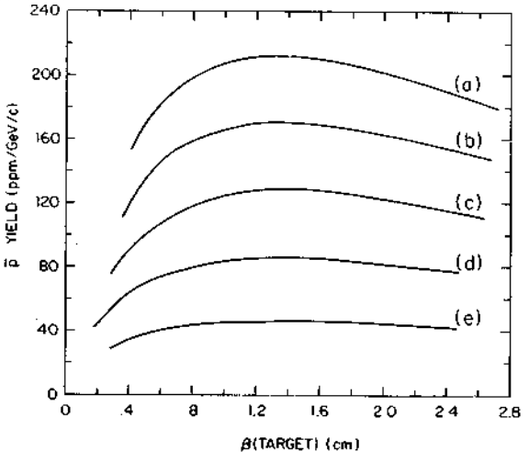

Fig. 7. Calculated variation in the pbar yield with β_0 (beta at the target center), for various acceptances: a = 30,25,20,15,10π mm-mrad for (a) through (e) respectively. Proton beam spot size σ_R = 0.54 mm, target length 5 cm.

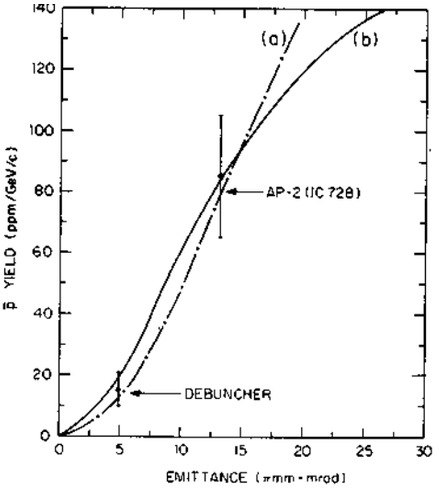

Fig. 8. Measured pbar yields in AP-2 and the Debuncher; curves are calculations of the expected yield vs emittance, for the operating conditions (σ_R = 0.42 mm, target length 7.2 cm): (a) lens gradient 600 T/m; (b) lens gradient 600 T/m.

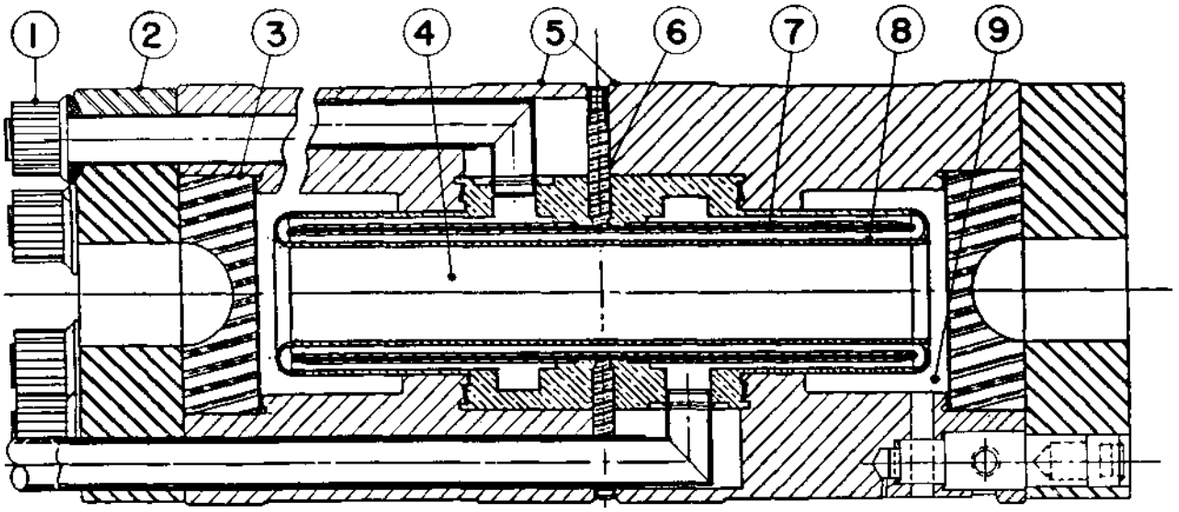

Fig. 5. Lithium lens prototype: 1-Retaining bolt;2-End flange;3-End caps; 4-Lithium; 5-Current contacts;6-Ceramic insulator;7-Water septum;8-Inner cooling jacket;9-Fill port.

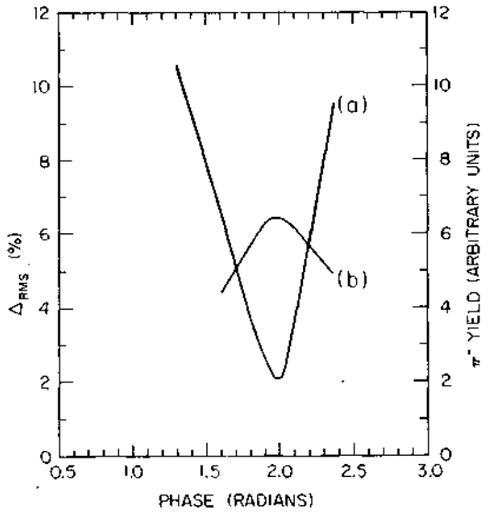

Fig. 9. (a) Calculated lens nonlinearity (defined in the text) vs. phase; (b) Measured pion yield in AP-2 (arbitrary scale) vs. phase at which the beam passes through the lens.

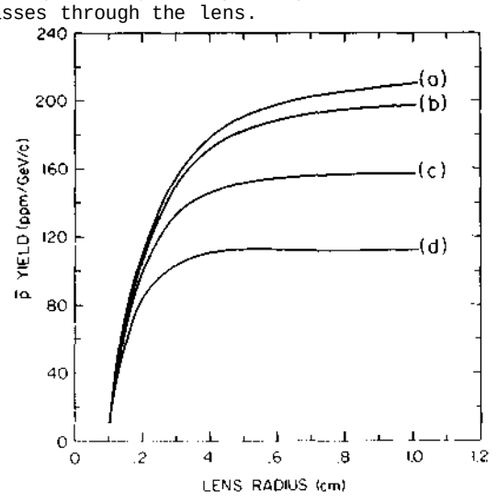

Fig. 10. Calculated dependence of the pbar yield on lens radius, with current scaling as I = 500(R_0/1 cm) kA, for various proton spot sizes: σ_R = 0,.2,.4,.6 mm for (a) through (d) respectively. Target length 5 cm, a = 20π mm-mrad.

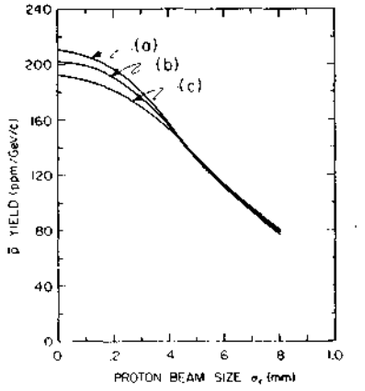

Fig. 11. Calculated dependence of the pbar yield on proton beam spot size, for various lens radii with current scaling as in fig. 10. (a) through (c) correspond to R_0 =10,7,5 mm respectively. Target length 5 cm, a = 20π mm-mrad.

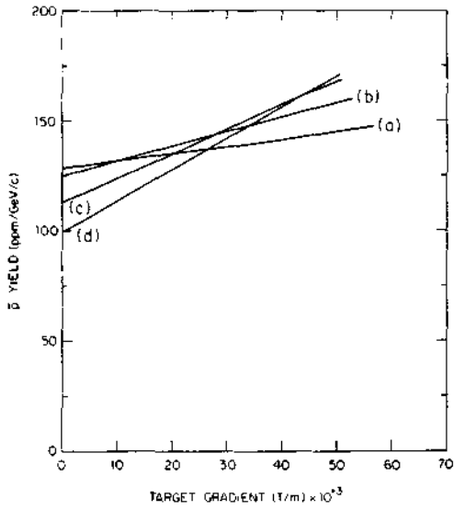

Fig. 12. Calculated dependence of the pbar yield on the gradient of a current-carrying tungsten target, for various target lengths: (a) through (d) correspond respectively to 5,7,9,11 cm. Acceptance ellipse aspect ratio picked for maximum yield. σ_R = .54 mm, a = 20π mm-mrad.